



HAL
open science

Number of spikes in single particle ICP-MS time scans: from the very dilute to the highly concentrated range

Pierre Emmanuel Peyneau, Martin Guillon

► **To cite this version:**

Pierre Emmanuel Peyneau, Martin Guillon. Number of spikes in single particle ICP-MS time scans: from the very dilute to the highly concentrated range. *Journal of Analytical Atomic Spectrometry*, 2021, 36 (11), pp.2460-2466. 10.1039/D1JA00156F . hal-03346976

HAL Id: hal-03346976

<https://hal.science/hal-03346976>

Submitted on 16 Sep 2021

HAL is a multi-disciplinary open access archive for the deposit and dissemination of scientific research documents, whether they are published or not. The documents may come from teaching and research institutions in France or abroad, or from public or private research centers.

L'archive ouverte pluridisciplinaire **HAL**, est destinée au dépôt et à la diffusion de documents scientifiques de niveau recherche, publiés ou non, émanant des établissements d'enseignement et de recherche français ou étrangers, des laboratoires publics ou privés.

Cite this: DOI: 00.0000/xxxxxxxxxx

Number of spikes in single particle ICP-MS time scans: from the very dilute to the highly concentrated range[†]

Pierre-Emmanuel Peyneau^{*a} and Martin Guillon^a

Received Date

Accepted Date

DOI: 00.0000/xxxxxxxxxx

The particle number concentration (PNC) of dilute nanoparticle dispersions can be determined by single particle inductively coupled plasma-mass spectrometry (sp-ICP-MS). Virtually equal to zero for very dilute dispersions, the difference between the number of nanoparticles having entered the plasma of the instrument and the number of detectable spikes in the time scan increases in a strongly nonlinear fashion with the PNC. This counting bias, which was unquantified yet, is due to particle event coincidences in the time scan and precludes at first sight the possibility to get meaningful information about the PNC of even moderately concentrated dispersions. In this article, we show that the counting bias is related to a stochastic process that models the spike occurrences in the time scan. This stochastic theory turns out to be amenable to analytic methods and yields universal predictions. We confirm their validity through Monte Carlo simulations and experiments with gold nanoparticle dispersions, for the full spectrum of PNC values we tested.

1 Introduction

There is a need in environmental science for size- and chemically sensitive analytical techniques able to provide direct information on the particle number concentration (PNC)^{1,2} of nanoparticle dispersions. Single particle inductively coupled plasma-mass spectrometry^{3–6} (sp-ICP-MS) meets these requirements and has been put forward over the last decade to analyze the presence of natural or engineered nanoparticles in the environment, on a particle per particle basis⁷.

The capacity of sp-ICP-MS to measure low PNCs is frequently underlined^{8,9}. It is one of the strengths of this technique for environmental nano-studies, where PNCs can be small. However, it is not always the case^{7,10}; dilution can be an option, but all dispersions are not stable with respect to dilution¹¹. Being able to directly analyze concentrated nanoparticle dispersions would be a very substantial improvement, as it would streamline the experimental workflow and alleviate concerns about the potential aggregation or disaggregation processes induced by dilution.

This study intends to overcome the low PNC constraint hindering the analytical potential of sp-ICP-MS^{6,12}. For very dilute dispersions of nanoparticles, the time-resolved signal – hereafter called time scan – measured by sp-ICP-MS is made of a sequence of spikes and the number of spikes is equal to the number of nanoparticles in very good approximation^{6,12,13}. This is no more

the case as the PNC increases: peaks related to different nanoparticles may overlap and the number of spikes can be much smaller than the number of nanoparticles having entered the plasma of the instrument¹². This counting bias, which was as yet unquantified, is currently detrimental to quantification of even moderately concentrated dispersions of nanoparticles. Taming the concentrated range is thus a major analytical challenge.

In this work, thanks to theoretical considerations supported by Monte Carlo simulations, we derive the mathematical relationship relating the average number of spikes to the average number of nanoparticles introduced in the plasma of an ICP-MS instrument. We then show that the strongly nonlinear equation we obtained theoretically and checked numerically fits very well the counting bias experimentally measured on gold nanoparticle dispersions, for a three orders of magnitude range of PNCs. We end with a discussion about our findings and their range of potential applications.

2 Theory and Monte Carlo simulations

When a nanoparticle dispersion is analyzed by sp-ICP-MS, nanoparticles enter randomly in the plasma with an average nanoparticle flux rate λ . If each particle contains a sufficient mass of the monitored isotope, a fraction of the ion cloud generated in the plasma will be detected, leading to a short-lived peak – hereafter called particle event – in the time scan. As demonstrated recently, the time sequence of ion clouds can be mapped to the points of discontinuity of a homogeneous Poisson process¹³. Consequently, the duration \mathcal{T} between two successive ion clouds (interarrival time) follows an exponential distribution

^a GERS-LEE, Univ Gustave Eiffel, IFSTTAR, F-44344 Bouguenais, France. E-mail: pierre-emmanuel.peyneau@univ-eiffel.fr

[†] Electronic Supplementary Information (ESI) available: [details of any supplementary information available should be included here]. See DOI: 00.0000/00000000.

with parameter λ ¹⁴, the probability density function (PDF) of this distribution being

$$\text{PDF}(\mathcal{F}) = \lambda e^{-\lambda t} \quad \text{for } t \geq 0. \quad (1)$$

In the very dilute limit where sp-ICP-MS experiments are performed in practice, statistically, almost all the particle events left by each ion cloud in the time scan are visible to the naked eye in the time scan. This is no longer the case when the PNC increases: indeed, the sequence of particle events stemming from each individual ion cloud is not necessarily discernable in the time scan when λ^{-1} has the same order of magnitude as the duration of particle events, that is typically equal to a few hundreds of microseconds^{6,15,16}. This guesstimate shows that, in sp-ICP-MS, the very dilute limit corresponds roughly to the range $\lambda < 100\text{s}^{-1}$, an estimate which is consistent with previous studies¹². When λ is larger, the counting bias – i.e. the difference between the number of particle events, which is equal to the number of nanoparticles having entered the plasma, and the number of spikes detectable in a time scan – becomes non-negligible.

However, it turns out that this brief analysis can be considerably refined. Step-by-step successive improvements will be the focus of the next subsections, allowing us to quantify analytically the average counting bias.

2.1 Zero dwell time and constant duration of particle events

For the sake of simplicity, we start by assuming that the duration of a particle event is constant and equal to τ_p and that the time scan signal is continuously sampled (this corresponds to a zero integration time, also called dwell time in mass spectrometry, hereafter denoted τ_{dw}). This situation is depicted in the left part of Fig. 1. Two individual particle events separated by a time interval greater than τ_p belong to two separated spikes; otherwise, they belong to the same (composite) spike. From Eq. 1, the time interval between the starts of two particle events has a probability $\text{Prob}(\mathcal{F} \geq \tau_p) = \int_{\tau_p}^{+\infty} \lambda e^{-\lambda t} dt = e^{-\lambda \tau_p}$ of being greater than τ_p . Each single nanoparticle is thus detectable with a probability $e^{-\lambda \tau_p}$. Since the average number of particles entering the plasma per unit of time is equal to λ , the average number of spikes $\langle N_s \rangle$ present in a time scan is given by

$$\langle N_s \rangle = \lambda e^{-\lambda \tau_p} \tau_{\text{obs}}, \quad (2)$$

where τ_{obs} is the duration of the sp-ICP-MS experiment. In the $\lambda \tau_p \rightarrow 0$ limit (very dilute limit in the terminology of Ref. 13), one gets $N_s = \lambda \tau_{\text{obs}}$ and we find ourselves in the theoretical framework worked out in Ref. 13.

Eq. 2 is reminiscent of mathematically analogous problems involving detector dead times, which are well documented for photon or ion counting and for the detection of nuclear events since the 1930s^{17–20}. Such questions have been recently studied in the sp-ICP-MS context²¹. There is a mathematical one-to-one correspondence – but not a physical one – between the pile-up problem we considered and dead time problems. We stress that we did not consider the dead time τ_{dead} of the detector in this work. Indeed, for electron multipliers, τ_{dead} is typically worth a few dozens of

nanoseconds^{21–23}, which is much less than τ_p . We thus neglected τ_{dead} in our analysis.

2.2 Zero dwell time and random duration of particle events

The duration τ of a particle event is related to the dispersion of the corresponding ion cloud during its transport within the instrument. A wealth of complex processes affect the fate of ion clouds in ICP-MS^{24–27}, hence some fluctuations of τ . Thus, in experiments, τ is not constant valued but can be modeled as a random variable. Fortunately, it turns out that Eq. 2 remains valid provided that one replaces τ_p by the average value of τ , denoted $\langle \tau \rangle$, whatever the probability distribution of τ is,

$$\langle N_s \rangle = \lambda e^{-\lambda \langle \tau \rangle} \tau_{\text{obs}}. \quad (3)$$

This result, which is both simple and quite surprising, is one of the keypoint of the present theoretical analysis. We are not aware of any elementary derivation of Eq. 3 for an arbitrary random variable τ . The most straightforward demonstration of this result relies on a branch of probability theory called renewal theory* (see for instance Ref. 29).

2.3 General theory: non-zero dwell time and random duration of particle events

Experimentally, due to electronics limitations, the dwell time cannot be strictly equal to zero. The continuous output signal generated by the instrument is thus discretized and is made up of multiple readings. This discretization entails some modifications of the theory, illustrated in the right part of Fig. 1. These are of importance in sp-ICP-MS because the duration of an ion cloud has the same order of magnitude as the minimum dwell time achievable on current generation instruments (a few hundreds of microseconds vs. a range of $10\mu\text{s}$ to a few milliseconds).

When $\tau_{\text{dw}} > 0$, compared to Eq. 3, an additional multiplicative factor appears in the mathematical expression of $\langle N_s \rangle$: the probability that there is no event over a duration $(2 - \{t/\tau_{\text{dw}}\})\tau_{\text{dw}}$, where $\{x\}$ denotes the fractional part of x , assuming that the current bin contains the end of the particle event associated with an ion cloud (the associated reading is thus nonzero). Let u denote $\{t/\tau_{\text{dw}}\}$; according to Eq. 1, the probability we just mentioned is equal to $\mathcal{P} = e^{-\lambda(2-u)\tau_{\text{dw}}}$. So the next reading is zero with probability \mathcal{P} and nonzero with probability $1 - \mathcal{P}$. However, u is itself a random variable following a uniform distribution on $[0, 1]$: indeed, according to Poisson process theory, assuming that there is an occurrence of a homogeneous Poisson process during a given time interval, the position of this occurrence is uniformly distributed on the interval¹⁴. Thus, the random variable $\mathcal{F}' = (2 - u)\tau_{\text{dw}}$ is uniformly distributed on the interval $[\tau_{\text{dw}}, 2\tau_{\text{dw}}]$, as shown in the lower part of the right panel of Fig. 1. Therefore, since u is uniformly distributed on $[0, 1]$, the average of \mathcal{P} is equal to $\int_0^1 e^{-\lambda(2-u)\tau_{\text{dw}}} du = e^{-2\lambda\tau_{\text{dw}}} (e^{\lambda\tau_{\text{dw}}} - 1) / (\lambda\tau_{\text{dw}})$. Multiplying this

* For the anecdote, there exists old links between this subfield of mathematics and analytical chemistry, since analytical questions stimulated some developments in renewal theory²⁸.

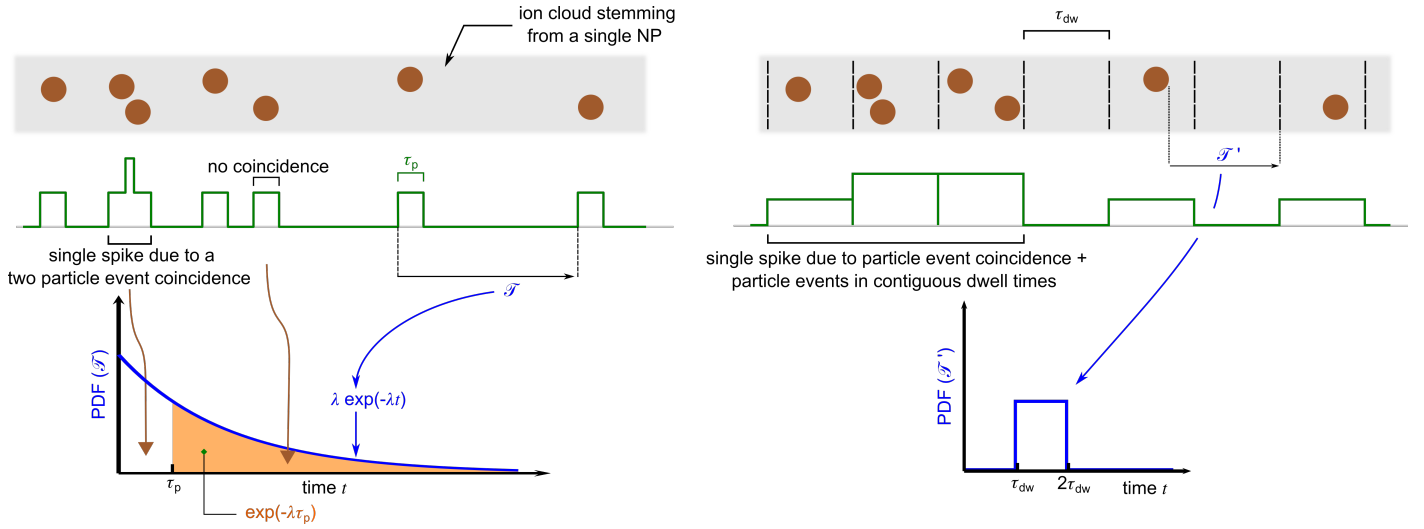


Fig. 1 Left panel: zero dwell time case. Each nanoparticle is transformed in an ion cloud by the plasma, and each ion cloud leaves a trace (called a particle event) of duration τ_p in the continuous time-resolved signal. Please note that the shape of the particle events is sketchy in this figure. Since the difference of time \mathcal{F} between the starts of two successive particle events is exponentially distributed, the probability that two particle events are well separated equals $e^{-\lambda\tau_p}$. In this part of the scheme, there are 7 nanoparticles but only 6 spikes. Right panel: nonzero dwell time case. When the dwell time is > 0 , the time-resolved signal is discretized, giving rise to the time scan, which is made up of discrete readings. In this case, even when two particle events are separated by a duration $> \tau_p$, they can belong to the same composite spike if they produce nonzero readings in adjacent time bins. For an ion cloud to be the last one of a given spike, the time difference between the end of the associated particle event and the end of the next time bin ought to be large enough. This time difference can be modeled through the random variable \mathcal{F}' , that can be shown to be uniformly distributed between τ_{dw} and $2\tau_{dw}$ (see main text). In this part of the scheme, there are 7 nanoparticles but only 3 spikes.

value by the r.h.s. term of Eq. 3, one gets for the average number of spikes in a time scan

$$\langle N_s \rangle = e^{-2\lambda\tau_{dw}} (e^{\lambda\tau_{dw}} - 1) e^{-\lambda\langle\tau\rangle} \tau_{obs}/\tau_{dw}. \quad (4)$$

This equation is the key result of our theoretical analysis. To our knowledge, it had never been established previously. As for Eq. 3, this result has a universal character in the sense that the average number of spikes does not depend on the shape of the probability distribution function of τ , but only on its average $\langle\tau\rangle$, which is a very fortunate property. Monte Carlo simulations ascertaining the validity of Eq. 4 for various probability distributions of τ are presented in Supplementary Information. They show excellent agreement between Eq. 4 and computer simulations.

The evolution of $\langle N_s \rangle$ as a function of λ for a $\tau_{obs} = 60s$ experiment is depicted in Fig. 2 for $\langle\tau\rangle = 300\mu s$ and $\langle\tau\rangle = 1000\mu s$, both for a zero and a $100\mu s$ dwell time. This 300-1000 μs range for $\langle\tau\rangle$ is consistent with values reported in the literature¹⁶. When $\lambda \leq 100s^{-1}$, $\langle N_s \rangle$ starts to increase linearly, but then, the curve quickly becomes concave, up to a maximum value reached when the nanoparticle flux entering the plasma equals $\lambda_{max} = \frac{1}{\tau_{dw}} \ln(1 + \frac{\tau_{dw}}{\langle\tau\rangle + \tau_{dw}})$. This maximum value is a rapidly decreasing function of $\langle\tau\rangle$. Then, $\langle N_s \rangle$ decreases and eventually tends towards 0: indeed, at one point, when λ is large enough, all the readings of the time scan are nonzero, and there is no more any detectable spike. Besides, Fig. 2 demonstrates that when λ is sufficiently large, $\langle N_s \rangle$ depends significantly both on $\langle\tau\rangle$ and τ_{dw} . Finally, Fig. 2 shows the excellent agreement between the average number of spikes predicted theoretically by Eq. 4 and calculated numerically by Monte Carlo simulation.

2.4 Stochastic process describing the spike count

Experimentally, the number of spikes detectable in a time scan is a random integer that fluctuates from one experiment to another. In the small λ limit (i.e. for very dilute nanoparticle dispersions), when both $\lambda\tau_{dw} \ll 1$ and $\lambda\langle\tau\rangle \ll 1$, the time sequence of spikes detectable in an experimental time scan can be mapped to the points of discontinuity of a homogeneous Poisson process¹³. In this limit, N_s thus follows a Poisson distribution. In addition, the Fano factor³⁰ F , which is defined as the ratio between the square of the spike count standard deviation to the mean, is equal to 1. As shown recently, all these predictions are in excellent agreement with experimental data¹³.

This is no longer true when $\lambda\langle\tau\rangle$ is not much less than 1. A non-negligible spike overlap entails some under-dispersion¹³. In this challenging but more general case, which is the focus of this study, N_s is still a discrete random variable, but according to renewal theory²⁹, when $\lambda\tau_{obs} \gg 1$, it follows in very good approximation a normal distribution whose mean value is given by Eq. 4. We indeed checked the normality of N_s (see Supplementary Information).

We remind that the expression of $\langle N_s \rangle$ is universal, in the sense that it depends on the probability density function of the particle event duration τ only through its average $\langle\tau\rangle$. This universal character does not hold for the standard deviation $\sigma(N_s)$ of the spike count. $\sigma(N_s)$, which is a measure of the fluctuations affecting N_s , can however be estimated by Monte Carlo simulation. Thanks to a dedicated program written in Python, we ran 10,000 simulations for different values of λ , assuming a constant duration τ_p for all the particle events. These calculations yield a lower bound for $\sigma(N_s)$ since it is even greater when the duration of particle

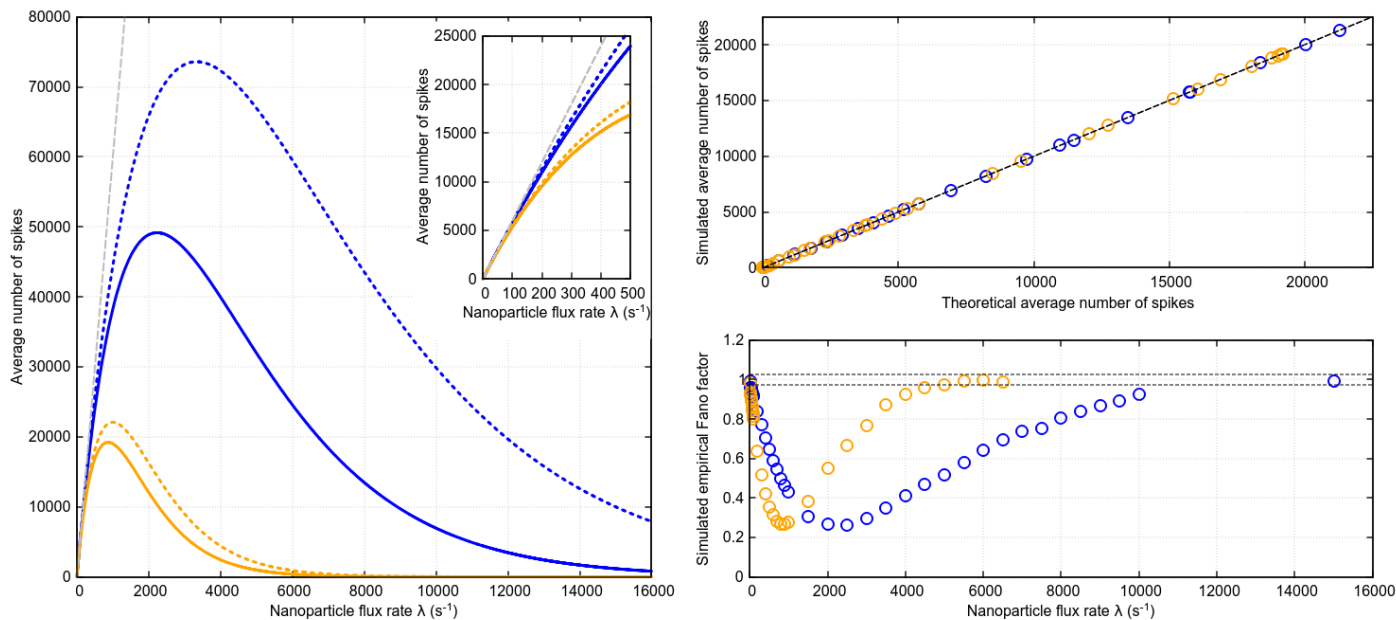


Fig. 2 Left: theoretical average number of spikes $\langle N_s \rangle$ as a function of the nanoparticle flux rate λ entering the plasma of the instrument, for $\langle\tau\rangle = 1000\mu\text{s}$ (orange curves) and $\langle\tau\rangle = 300\mu\text{s}$ (blue curves), each time with $\tau_{\text{dw}} = 100\mu\text{s}$ (plain lines —) and a zero dwell time (dotted lines \cdots). The gray dashed line (---) would be the average number of spikes in the time scan if each nanoparticle was detectable. The inset figure is a zoom on the range $\lambda < 500\text{s}^{-1}$. Top right: comparison between the simulated and theoretical average number of spikes in a time scan. Orange circles \circ correspond to $\langle\tau\rangle = 1000\mu\text{s}$ and blue circles \circ to $\langle\tau\rangle = 300\mu\text{s}$. The dashed line is here to guide the eye. Bottom right: empirical Fano factor \hat{F} calculated by Monte Carlo simulation for different nanoparticle flux rates λ , both with $\langle\tau\rangle = 1000\mu\text{s}$ (orange circles \circ) and $\langle\tau\rangle = 300\mu\text{s}$ (blue circles \circ). The two dashed horizontal lines correspond to the lower (0.972) and upper (1.028) bounds of the 95% confidence interval for \hat{F} when it is calculated from 10,000 independently drawn values (see main text).

events is a random variable with a nonzero variance: in this case, there is an overdispersion due to the fluctuations of τ itself.

Given the expected Poissonity of the spike count in the very dilute limit, we plotted in Fig. 2 the empirical Fano factor \hat{F} – square of the empirical standard deviation divided by the empirical mean – instead of the empirical standard deviation, obtained from 10,000 randomly generated synthetic time scans, for $\tau_p = 300\mu\text{s}$ and $\tau_p = 1000\mu\text{s}$, with a $100\mu\text{s}$ dwell time.

As expected, Fig. 2 shows that the empirical Fano factor is very close to 1 when λ is small enough. For the smallest value we simulated ($\lambda = 10\text{s}^{-1}$), \hat{F} even belongs to the 95% confidence interval of this estimator, [0.972, 1.028], that can be calculated from the Gamma approximation to the sampling distribution of F^{31} . Once again, it is an illustration of the Poissonian character of the spike count in the very dilute limit. \hat{F} starts to decrease when λ increases, reaches a minimum value, and then increases again up to a value close to 1, belonging to the 95% confidence interval, suggesting the existence of an underlying homogeneous Poisson process in the very concentrated range[†].

In any case, given the definition of the Fano factor, the empirical standard deviation is equal to $(\hat{F} \langle N_s \rangle)^{1/2}$. Since $\hat{F} \leq 1$ whatever λ is worth, the coefficient of variation $\sigma(N_s)/\langle N_s \rangle$ of the number of spikes is always smaller than $\langle N_s \rangle^{-1/2}$. The probability distribution of N_s is thus fairly narrow; for instance, $\sigma(N_s)/\langle N_s \rangle \leq 1/10$ as soon as $\langle N_s \rangle \geq 100$.

3 Experimental validation

3.1 Instrument and settings

The sp-ICP-MS experiments were conducted with a Agilent 8900 ICP-MS-QQQ mass spectrometer, equipped with a Micromist concentric nebulizer and a Scott double pass spray chamber. The uptake flow rate was set to 0.346mLmin^{-1} . The measured isotope was ^{197}Au . Each measurement was performed during $\tau_{\text{obs}} = 60\text{s}$ with a zero settling time. Finally, the dwell time τ_{dw} was set to $100\mu\text{s}$ or $300\mu\text{s}$. The operating parameters of the instrument are given in Supplementary Information.

3.2 Experimental protocol and samples

Experiments were performed with dispersions of 60nm gold nanoparticles stabilized with a citrate buffer, purchased from Sigma-Aldrich. The stock dispersion, whose PNC $\approx 1.9 \times 10^{10}\text{mL}^{-1}$, was shaken and ultrasonicated during 1min before being diluted with several dilution factors: 250000, 7500, 3750,

the unit Fano factor found by Monte Carlo simulation.

[†]This result is surprising at first sight. Indeed, Poissonity is expected to be destroyed as the particle events start to overlap. However, there is a kind of duality at play: while the starts of the non-zero readings blocks can be mapped to the points of discontinuity of a homogeneous Poisson process when λ is small enough, the starts of the zero reading blocks can in turn be mapped to the points of discontinuity of a homogeneous Poisson process when λ is sufficiently large. Since the number of non-zero reading blocks is equal to the number of zero reading blocks in a time scan, it implies that N_s once again follows a Poisson distribution when λ is large, hence

2500, 1875, 1500, 1250, 1071, 938, 833, 750, 682, 625, 577, 536, 500 and 250. For both values of the dwell time (100 and 300 μs), each diluted sample was analyzed three times by sp-ICP-MS.

3.3 Time scan processing

Spikes were extracted from the time scans with a custom-written Python program. In this work, a spike was defined as a sequence of nonzero readings in a time scan. The number of such sequences in a time scan is called the total spike count. By definition, each spike is immediately preceded and followed by a zero reading: between these zero readings at both ends of a single spike, all the readings of a single spike have to be nonnegative.

However, experimental time scans are affected by a small level of noise. To properly extract the spike count of a given experimental time scan, one has to remove the noisy spikes stemming from the noise affecting the zero baseline. In our study, we assimilated the level of noise to the highest value among all the spikes that lasted only during a single reading in the time scans measured on the most dilute samples ($250,000\times$ dilution factor). A spike was considered as noisy when its summed intensity divided by its temporal width was smaller than the level of noise found previously from the $250,000\times$ diluted samples.

Finally, the spike count was defined as the difference between the total spike count and the number of noisy spikes. We underline that this counting method is very simple and generic since we only processed the readings according to their zero/nonzero status: we did not make any assumption on the shape, the intensity or the duration of a spike.

The method we employed to determine the spike count of a time scan is crucial for agreement with the theory. It differs from the standard one, where an iterative algorithm is used to determine a threshold value above which the signal is considered as stemming from a nanoparticle⁵. It turns out that this latter method is not well suited to the data processing of time scans produced by concentrated dispersions. Indeed, in this case, the overlap of many particle events generates a kind of effective background which may be confused with a nonzero dissolved background when the traditional approach is used. A comparison between both methods is provided in Supplementary Information to illustrate this point.

3.4 Comparison with theory

The spikes were counted for all the experimental time scans. We had three different time scans for every dilution factor and we calculated the corresponding mean spike count.

The nanoparticle flux rate was estimated from the dilution factors and the number of spikes measured for the dispersion with the highest dilution factor (250,000 in our experiments). Given the PNC of the stock solution and the instrument settings, the $250,000\times$ diluted dispersion was very dilute with respect to sp-ICP-MS¹³. We were thus in the linear part of Fig. 2, where the spike count is equal to the number of nanoparticles having entered the plasma during the experiment in very good approximation. We thus inferred the nanoparticle flux rate $\lambda_{250,000}$

when $d_f = 250,000$. From this value, assuming that the transport efficiency⁵ remained the same regardless d_f , we deduced the nanoparticle flux rate for the other solutions through $\lambda_{d_f} = \lambda_{250,000} \times 250000/d_f$.

However, this estimation is not very accurate because of the counting fluctuations affecting the spike count and the existence of a small systematic counting bias due to the little probability of particle event overlap¹². In the very dilute regime, the empirical Fano factor is equal to 1, meaning that the relative counting fluctuations affecting N_s are equal to $1/\langle N_s \rangle$. Since we detected ≈ 1000 spikes in the time scans for the $250,000\times$ diluted dispersion, according to the normal approximation to the Poisson distribution, the relative uncertainty affecting $\lambda_{250,000}$ is comprised between 0.905 and 1.095 with a 99.7% level of confidence. This level of uncertainty is a genuine problem to compare the experimental results with the theory, because the factor $250000/d_f$ can be very large – up to 10^3 for $d_f = 250$ – which is a source of propagating errors.

To circumvent this issue, we considered $\lambda_{250,000}$ as a first guess that needed to be slightly refined. Using the Levenberg-Marquardt algorithm³², we numerically fitted the mean number of spike counts detected in the experimental time scans to the following two-parameter objective function,

$$f_{\text{obj}} : (\langle \tau \rangle, \delta) \mapsto e^{-2\delta\lambda\tau_{\text{dw}}} (e^{\delta\lambda\tau_{\text{dw}}} - 1) e^{-\delta\lambda\langle \tau \rangle} \tau_{\text{obs}}/\tau_{\text{dw}}. \quad (5)$$

The raison d'être of parameter δ is to compensate for the uncertainty affecting $\lambda_{250,000}$, which is related to the counting fluctuations and the possible small systematic counting bias we discussed.

The minimization of the residual sum of squares yields $\delta = 1.091$ and $\langle \tau \rangle = 803.4 \mu\text{s}$ for the time scans measured with $\tau_{\text{dw}} = 100 \mu\text{s}$, and $\delta = 1.027$ and $\langle \tau \rangle = 807.7 \mu\text{s}$ for the time scans measured with $\tau_{\text{dw}} = 300 \mu\text{s}$. As expected from a statistical viewpoint, the δ values are within the range [0.905, 1.095]. The $\langle \tau \rangle$ values inferred from the $\tau_{\text{dw}} = 100 \mu\text{s}$ and $\tau_{\text{dw}} = 300 \mu\text{s}$ sp-ICP-MS experiments are very close to each other (803.4 vs. 807.7 μs), confirming the accuracy and the robustness of the theoretical model.

The mean spike counts extracted from the experimental time scans and the corresponding nanoparticle flux rates, corrected for the δ values found through the optimization procedure, are reported in Fig. 3, with the numerical adjustments. We used the mean value $\langle \tau \rangle = 805.5 \mu\text{s}$ for both fits. Both adjustments appear to be very good, despite the strong nonlinearity of the theoretical model.

3.5 Experimental data-driven Monte Carlo simulations

We finally ran some Monte Carlo simulations with a constant valued duration for the particle events, equal to $805.5 \mu\text{s}$. The three-fold standard deviations calculated from 10,000 runs are reported in Fig 3. As explained in the theory section, these values are lower bounds since the particle event duration is not constant valued in the experiments.

Experimentally, the average spike duration measurable from a time scan is necessarily greater than $\langle \tau \rangle$ because of the discretization of the time scan. When $\langle \tau \rangle = 805.5 \mu\text{s}$ and for $\tau_{\text{dw}} = 100 \mu\text{s}$,

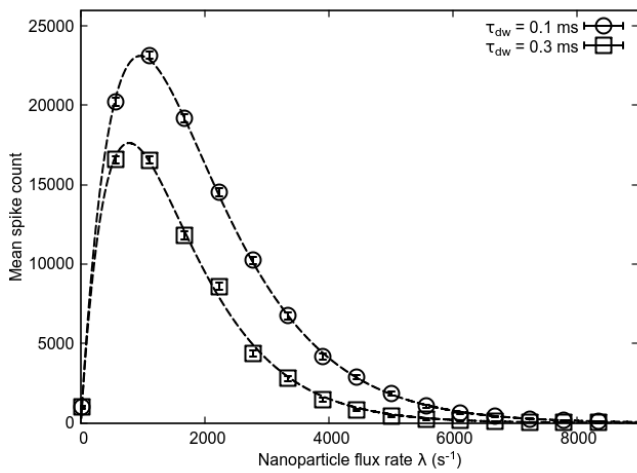


Fig. 3 Mean spike counts extracted from the experimental time scans for $\tau_{\text{dwell}} = 100 \mu\text{s}$ (circle symbols) and $\tau_{\text{dwell}} = 300 \mu\text{s}$ (square symbols). The dashed lines are the numerical adjustments to the model (Eq. 4) with the same value for the average duration of a particle event, $\langle\tau\rangle = 805.5 \mu\text{s}$. The three-sigma error bars associated with each data point were computed by Monte Carlo simulation.

Monte Carlo calculations yield an average spike duration equal to $910 \mu\text{s}$ for $\lambda = 10 \text{s}^{-1}$. This duration agrees very well with a value ($906 \mu\text{s}$) reported previously for 60 nm gold nanoparticles¹⁶.

The difference between the average spike duration and the average particle event duration should vanish when τ_{dwell} tends towards 0. For the record, with $\tau_{\text{dwell}} = 10 \mu\text{s}$, a value currently achievable with a few current-generation ICP-MS, Monte Carlo simulations yield an average spike duration of $819 \mu\text{s}$, a value much closer to $\langle\tau\rangle = 805.5 \mu\text{s}$ than when $\tau_{\text{dwell}} = 100 \mu\text{s}$.

4 Discussion

Eq. 4 gives a quantitative estimate for the counting bias, i.e. the difference between the number of spikes detectable in a time scan and the number of nanoparticles having entered the plasma. The existence of this counting bias and its impact on sp-ICP-MS measurements had already been reported¹², even in the case of dilute nanoparticle dispersions, but to our knowledge, it had never been accurately quantified yet.

Since $\langle N_p \rangle = \lambda \tau_{\text{obs}}$ is the average number of particles entering the plasma of the instrument during an sp-ICP-MS experiment, Eq. 4 yields

$$\langle N_s \rangle = e^{-2\lambda\tau_{\text{dwell}}} \frac{e^{\lambda\tau_{\text{dwell}}} - 1}{\lambda\tau_{\text{dwell}}} e^{-\lambda\langle\tau\rangle} \langle N_p \rangle. \quad (6)$$

This relationship is strongly nonlinear when $\lambda\langle\tau\rangle$ or/and $\lambda\tau_{\text{dwell}}$ are not much less than 1. This nonlinearity stems from: i) the possible overlap related to the finite duration of particle events; ii) the discrete sampling of the continuous signal delivered by the instrument each dwell time. These two sources of counting bias are independent of each other, hence the two multiplicative terms in Eq. 6, $e^{-\lambda\langle\tau\rangle}$ and $e^{-2\lambda\tau_{\text{dwell}}} (e^{\lambda\tau_{\text{dwell}}} - 1) / (\lambda\tau_{\text{dwell}})$, the former depending only on $\langle\tau\rangle$ and the latter only on τ_{dwell} .

In the sp-ICP-MS context, both origins of counting bias are of

importance since $\langle\tau\rangle$ and τ_{dwell} values are similar or differ at most by one order of magnitude. In any case, this is not enough for one source of bias to grossly dominate the other and both origins have to be taken into account simultaneously.

This would not necessarily be the case with a different analytical technique. Indeed, the theory we devised is not restricted to sp-ICP-MS. It could be applied to any analytical method where discrete “objects” (be they cells, molecules, or micro- or nanoparticles) enter randomly within an instrument and leave a short-lived peak (trace), well above the baseline, in a time sampled continuous one-dimensional output signal (e.g. a current trace in resistive pulse sensing). Depending on the product of the sampling rate f by the mean duration $\langle\tau\rangle_{\text{peak}}$ of a “object” event, one source of nonlinearity can be predominant. If $f \times \langle\tau\rangle_{\text{peak}} \ll 1$, the sampling bias prevails; if $f \times \langle\tau\rangle_{\text{peak}} \gg 1$, the overlapping bias dominates; finally, if $f \times \langle\tau\rangle_{\text{peak}} \approx 1$, as in sp-ICP-MS, neither the sampling nor the overlapping bias can be neglected.

Going back to sp-ICP-MS, one may wonder whether the theory remains valid when the nanoparticles have an arbitrary probability size distribution. Indeed, the particle event duration corresponding to a single particle is known to be correlated to the size of the nanoparticle¹⁶. However, since Eq. 4 is applicable regardless of the probability distribution of the spike duration, we expect the theory to hold for every possible mixture of nanoparticles of different sizes, with the polydispersity affecting solely the value of the mean peak duration $\langle\tau\rangle$. We checked successfully this theoretical prediction on a mixture of 60 and 150 nm-sized nanoparticles (see Supplementary Information).

5 Conclusion

In this study, we derived theoretically and checked numerically and experimentally the mathematical relationship between the average number of spikes $\langle N_s \rangle$ in a sp-ICP-MS time scan and the average number of nanoparticles $\langle N_p \rangle$ entering the ICP. The nonlinear relationship we obtained is very accurate and robust. In particular, it does not depend on the shape of the distribution of particle event durations, but only on its average. It is also insensitive to the nonlinearities (e.g. detector saturation) potentially induced by the pile-up of particle events. Because of these properties, the theory presented in this work holds whatever the particle size distribution of the nanoparticles in solution.

Experimentally, the relationship we unveiled is valid regardless the value of the nanoparticle flux rate λ . It holds on three orders of magnitude – from $\lambda \approx 10$ to $\approx 10^4 \text{s}^{-1}$ – which is the maximum achievable dynamic range of the sp-ICP-MS technique from a practical viewpoint. To our knowledge, such a dynamic range had never been quantitatively explored so far in sp-ICP-MS.

From a practical viewpoint, the theory allows the accurate quantification of the counting bias induced by the combination of the finite duration of a particle event and the nonzero value of the dwell time. This systematic bias is present even with dilute dispersions and had never been so thoroughly studied yet.

We also think the theory we devised is a significant step forward regarding the analysis of moderately to highly concentrated dispersions of nanoparticles. It paves the way for the determination of the particle number concentration of such dispersions, since

it relates a detectable quantity – the spike count – to a number which is relevant from an analytical point of view – the number of particles having entered the ICP. To move towards this stimulating direction, besides the relationship between $\langle N_s \rangle$ and $\langle N_p \rangle$ derived in this study, we still need i) a good knowledge of the whole probability distribution of the number of spikes N_s ; ii) a way to extract an accurate value of the average duration of a particle event $\langle \tau \rangle$ from a time-resolved signal whose integration time is often only slightly smaller than typical $\langle \tau \rangle$ values in sp-ICP-MS; iii) to deal with the fact that two very different values of the nanoparticle flux rate can yield the same average number of spikes; iv) to cope with a possible nonzero value of the background signal, due to for instance the presence of a substantial amount of the monitored element under dissolved form, or interferences. Once these issues will have been settled, provided that the transport efficiency is accurately known, the necessary ingredients to quantify the particle number concentration of nanoparticle dispersions of arbitrary concentration by sp-ICP-MS will be available.

Finally, the theory in its present shape is focused on the particle number concentration. It does not allow the recovery of other valuable information that are available when performing traditional sp-ICP-MS measurements on very dilute dispersions, such as the probability distribution of the mass of the monitored element in each particle. Finding a way to overcome this obstacle would be a nice achievement.

Conflicts of interest

There are no conflicts to declare.

Acknowledgements

We thank Jérôme Raimbault for preliminary discussions about sp-ICP-MS and Émilie Faillard for discussions on the manuscript.

This research was supported by the French National Research Agency (grant no. ANR-17-CE04-010).

Code availability

The Python programs written to perform the Monte Carlo simulations and to process the experimental sp-ICP-MS data are available at <https://git.io/JEiQC>.

Author contributions

PEP worked out the theory, wrote the computer programs, ran the numerical simulations, processed the data and wrote the article. MG performed the sp-ICP-MS experiments.

Notes and references

- 1 M. F. Hochella, D. W. Mogk, J. Ranville, I. C. Allen, G. W. Luther, L. C. Marr, B. P. McGrail, M. Murayama, N. P. Qafoku, K. M. Rosso *et al.*, *Science*, 2019, **363**, year.
- 2 G. E. Batley, J. K. Kirby and M. J. McLaughlin, *Accounts of chemical research*, 2013, **46**, 854–862.
- 3 C. Degueldre and P. Favarger, *Colloids and Surfaces A: Physicochemical and Engineering Aspects*, 2003, **217**, 137–142.
- 4 F. Laborda, J. Jiménez-Lamana, E. Bolea and J. R. Castillo, *Journal of Analytical Atomic Spectrometry*, 2011, **26**, 1362–1371.
- 5 H. E. Pace, N. J. Rogers, C. Jarolimek, V. A. Coleman, C. P. Higgins and J. F. Ranville, *Analytical Chemistry*, 2011, **83**, 9361–9369.
- 6 J. W. Olesik and P. J. Gray, *Journal of Analytical Atomic Spectrometry*, 2012, **27**, 1143–1155.
- 7 M. Hadioui, G. Knapp, A. Azimzada, I. Jreije, L. Frechette-Viens and K. J. Wilkinson, *Analytical chemistry*, 2019, **91**, 13275–13284.
- 8 F. Laborda, E. Bolea and J. Jiménez-Lamana, *Analytical Chemistry*, 2014, **86**, 2270–2278.
- 9 M. D. Montañó, J. W. Olesik, A. G. Barber, K. Challis and J. F. Ranville, *Analytical and bioanalytical chemistry*, 2016, **408**, 5053–5074.
- 10 T. Erhardt, C. M. Jensen, O. Borovinskaya and H. Fischer, *Environmental science & technology*, 2019, **53**, 13275–13283.
- 11 J. Wan, Y. Kim, M. J. Mulvihill and T. K. Tokunaga, *Environmental toxicology and chemistry*, 2018, **37**, 1301–1308.
- 12 I. Abad-Álvarez, E. Peña-Vázquez, E. Bolea, P. Bermejo-Barrera, J. R. Castillo and F. Laborda, *Analytical and bioanalytical chemistry*, 2016, **408**, 5089–5097.
- 13 P.-E. Peyneau, *Spectrochimica Acta Part B: Atomic Spectroscopy*, 2021, **178**, 106126.
- 14 J. F. C. Kingman, *Poisson processes*, Clarendon Press, Oxford, 1993.
- 15 O. Borovinskaya, S. Gschwind, B. Hattendorf, M. Tanner and D. Günther, *Analytical chemistry*, 2014, **86**, 8142–8148.
- 16 J. Fuchs, M. Aghaei, T. D. Schachel, M. Sperling, A. Bogaerts and U. Karst, *Analytical chemistry*, 2018, **90**, 10271–10278.
- 17 H. Volz, *Zeitschrift für Physik*, 1935, **93**, 539–542.
- 18 L. Schiff, *Physical Review*, 1936, **50**, 88.
- 19 T. Graf, *Journal de Physique et Le Radium*, 1939, **10**, 513–518.
- 20 J. Ingle and S. Crouch, *Analytical chemistry*, 1972, **44**, 777–784.
- 21 I. Strengé and C. Engelhard, *Journal of Analytical Atomic Spectrometry*, 2020, **35**, 84–99.
- 22 A. J. Fahey, *Review of scientific instruments*, 1998, **69**, 1282–1288.
- 23 S. M. Nelms, C. R. Quétel, T. Prohaska, J. Vogl and P. D. Taylor, *Journal of Analytical Atomic Spectrometry*, 2001, **16**, 333–338.
- 24 A. Bogaerts and M. Aghaei, *Journal of Analytical Atomic Spectrometry*, 2017, **32**, 233–261.
- 25 O. Borovinskaya, M. Aghaei, L. Flamigni, B. Hattendorf, M. Tanner, A. Bogaerts and D. Günther, *Journal of Analytical Atomic Spectrometry*, 2014, **29**, 262–271.
- 26 I. I. Stewart and J. W. Olesik, *Journal of the American Society for Mass Spectrometry*, 1999, **10**, 159–174.
- 27 G. C.-Y. Chan and G. M. Hieftje, *Spectrochimica Acta Part B: Atomic Spectroscopy*, 2016, **121**, 55–66.
- 28 J. Hammersley, *Mathematical Proceedings of the Cambridge Philosophical Society*, 1953, pp. 623–637.
- 29 W. L. Smith, *Mathematical Proceedings of the Cambridge Philosophical Society*, 1957, pp. 175–193.

- 30 U. Fano, *Physical Review*, 1947, **72**, 26–29.
- 31 U. T. Eden and M. A. Kramer, *Journal of Neuroscience Methods*, 2010, **190**, 149–152.
- 32 W. H. Press, S. A. Teukolsky, W. T. Vetterling and B. P. Flannery, *Numerical Recipes: The Art of Scientific Computing*, Cambridge University Press, 2007.